Hindawi
Wireless Communications and Mobile Computing
Volume 2023, Article ID 1613190, 12 pages
https://doi.org/10.1155/2023/1613190

Research Article

Ergodic Capacity for NOMA-Enabled ISATNs with Transmit Antenna Selection and Imperfect CSI and SIC

Haifeng Shuai, Kefeng Guo, and Shibing Zhu

School of Space Information, Space Engineering University, Beijing 101407, China

Correspondence should be addressed to Kefeng Guo; guokefeng.cool@163.com and Shibing Zhu; sbz_zhu@sohu.com

Received 5 September 2022; Revised 31 October 2022; Accepted 25 November 2022; Published 6 February 2023

Academic Editor: Yanpeng Dai

Integrated satellite-aerial-terrestrial networks (ISATNs) expand the breadth and depth of seamless connections, which has been recognized as one of the key facilities of next-generation networks. This paper investigates the impact of transmit antenna selection, imperfect channel state information (CSI), and successive interference cancellation (SIC) on ergodic capacity (EC) of nonorthogonal multiple access- (NOMA-) enabled ISATNs, where a high altitude platform (HAP) assists the satellite transmission through decode-and-forward relaying protocol. Besides, two selection schemes are proposed to balance system complexity and transmission efficiency. Imperfect CSI and SIC are considered to impose detrimental effects on system performance. In addition, analytical expressions for EC of NOMA-enabled ISATNs in the presence of the above imperfections are derived. Finally, the Monte Carlo simulations corroborate analytical results and reveal the impacts of imperfections on integrated satellite-aerial-terrestrial networks.

1. Introduction

Integrated satellite-aerial-terrestrial networks (ISATNs) have been considered as an indispensable component in next generation wireless communication systems to service remote areas and improve users service quality [1, 2]. However, ISATNs require a vast amount of spectrum resources to be in service of a large amount of data and massive users. Under this condition, nonorthogonal multiple access (NOMA) scheme is introduced into ISATNs [3, 4]. NOMA scheme adopts power domain access to serve multiple users with the same resource block, thus it can enhance the spectral efficiency of the wireless systems compared to orthogonal multiple access (OMA) scheme [5–7]. Under the urgent demands for high spectrum efficiency and ubiquitous connectivity, the NOMA-enabled ISATN has bright foreground.

1.1. Related Works. The explosive growth of wireless access requirements for large-scale access users in a wide coverage range put forward high requirements for the current terrestrial network [8]. On this basis, the aerial networks, satellite networks, and current terrestrial network are combined, that is, integrated satellite-aerial-terrestrial networks [9]. The research in ISATNs has attracted global attention from academia and industry. In [10], two unmanned aerial vehicles (UAVs) were deployed as decode-and-forward (DF) relays to assist the communications of two terrestrial users, where outage probability (OP) was derived to validate the performance of system. The authors of [11] analyzed the outage performance of a cooperative satellite-aerial-terrestrial network, and the exact and asymptotic expressions for OP were obtained. In [12], two classical cooperative protocols, i.e., amplify-and-forward (AF) and DF were compared in a downlink hybrid satellite-terrestrial relay network by deriving the accurate expression of secrecy outage probability. Ergodic capacity (EC) is another important performance metric for the wireless network. In [13], the authors obtained the closed form expressions for OP and EC of an integrated satellite-terrestrial relay network to reveal the performance of the considered system.

Due to the scarcity of spectrum resources, the application of NOMA scheme, which can serve multiusers simultaneously, is necessary to improve the resource utilization of

wireless networks [14]. In a two-way relay NOMA system, the authors of [15] analyzed the outage behavior and ergodic rates of the system. In [16], the reliability and security of an ambient backscatter NOMA system were analyzed by deriving the expression of OP and intercept probability. The authors of [17] introduced NOMA scheme in hybrid satellite-terrestrial relay networks, so that the performance of OP was enhanced. The authors of [18] compared NOMA with OMA in an underlay cognitive hybrid satellite-terrestrial and verified the superiority of NOMA.

Multiple-antenna technique is widely deployed in wireless communication system to improve the transmission diversity [19]. On the other hand, multiple-antenna scenario brings greater overhead and system complexity, and even waste resources [20]. Therefore, in order to balance system performance and complexity, transmit antenna selection (TAS) was proposed [21]. In this regard, it is necessary to adopt TAS scheme in the ISATN with multiple-antenna. In [22], the authors have studied the outage behavior of the integrated satellite-HAP-terrestrial network. The authors of [23] analyzed the antenna selection scheme in a multiantenna two-way relay system, and OP was derived to evaluate the performance of the system.

Owing to the severe channel fading, it is hard to acquire perfect channel state information (CSI), and channel estimation errors (CEEs) arise during channel estimation process [24]. In [25], the impact of CEEs on the performance for spectrum sharing DF multiple-relay network was analyzed. The authors of [26] investigated the impact of imperfect CSI on cooperative NOMA system, and novel closed-form and asymptotic expressions for the OP, EC, and energy efficiency (EE) were derived. In addition, successive interference cancellation (SIC) in NOMA scheme may not decode the superimposed signal perfectly as a result of errors due to poor synchronization and propagation receiver [27]. In [28], imperfect SIC was considered to obtain the adaptive power allocation coefficient in a cooperative full duplex NOMA system. In [29], the authors obtained the secrecy outage probability for a unified NOMA framework under perfect SIC and imperfect SIC to analyze the physical layer security of NOMA system.

1.2. Research Gap and Contributions. The previous paper of us [30] is the first in open technical papers that investigated the joint effect of imperfect CSI and SIC on the performance of land mobile satellite system. Different from [30], in this paper, a HAP which works as an aerial half-duplex decode-and-forward (DF) relay is employed in the system and the TAS scheme is adopted at the transmitter of HAP. Try the authors' best knowledge, there is no prior work that analyzed the ergodic capacity (EC) for NOMA-enabled ISATNs with TAS scheme and imperfections.

Inspired by the aforementioned observations, in this paper, EC of NOMA-enabled ISATN with TAS schemes and imperfect CSI and SIC is investigated. Particularly, our main contributions are summarized as follows:

(1) Firstly, considering the characteristics of HAP, a novel architecture of NOMA-enabled integrated-satellite-aerial-terrestrial network is established, where the HAP is employed as a half-duplex DF relay to assist the transmission between satellite and user

(2) Secondly, on the foundation of imperfect CSI and SIC, the transmit antenna selection schemes based on the quality of service of different users are proposed. Moreover, the channel responses of Nakagami-m fading and shadowed-Rician (SR) fading under multiantenna and TAS schemes are derived

(3) Finally, the expressions of EC for NOMA-enabled ISATN under TAS schemes and imperfections are evaluated by utilization of Meijer-G functions. Numerical simulations are demonstrated to validate the preponderance of the considered system

1.3. Organization. The rest of this paper is organized as follows. In Section II, the system model and problem formulation are discussed. Then, the TAS schemes and EC are obtained in Section III. In Section IV, Monte Carlo simulations are given to reveal the performance of the considered system. Finally, the conclusions are included in Section V.

Notations: $E(\cdot)$ represents the expectation. $|\cdot|$ denotes the absolute value. $(p)_k$ represents the Pochhammer symbol ([31], p.xliii). $\Gamma(\cdot)$ is gamma function ([31], 8.310.1). $G_{p,q}^{m,n}(\cdot|\cdot)$ represents Meijer-G function ([31], 9.301).

2. System Model and Problem Formulation

As shown in Figure 1, we consider a power domain NOMA-enabled ISATN, which comprises a geosynchronous earth orbit (GEO) satellite (S), a HAP which works as an aerial DF relay (HAP is quasi-stationary suspended at an altitude of 20 km, hence, the impacts of the scattering and multipath are low.), and two terrestrial users (U_i), $i \in \{1, 2\}$ (Two-user group NOMA situation has the authentication of the Third Generation Partnership Project (3GPP), which can improve the spectrum efficiency of the system. Meanwhile, the derivations in this paper can be extended to any NOMA pair with more users [7]). Due to the high buildings, heavy fading, and other obstacles, thus terrestrial users cannot directly receive the satellite signal. Hence, HAP works as a relay which receives and forwards the satellite signal to destinations. It is assumed that the aerial relay and terrestrial destinations are located in the same identical GEO satellite beam. Moreover, HAP uses N_r receive antennas and N_t transmit antennas to form a uniform planar array (UPA), which can improve array gain. In addition, the terrestrial destinations are assumed to be small devices, such as IoT sensors, whose structures can only deploy single antenna [30, 32].

2.1. Signal Model. The whole transmission comprises two time slots. In the first time slot, the GEO satellite broadcasts a superimposed signal to the HAP which is given by

$$s = \sqrt{a_1}x_1 + \sqrt{a_2}x_2, \tag{1}$$

where x_i denotes the target signal of two terrestrial users U_i, obeying $E(|x_i|^2) = 1$. In NOMA scheme, a_i represents the

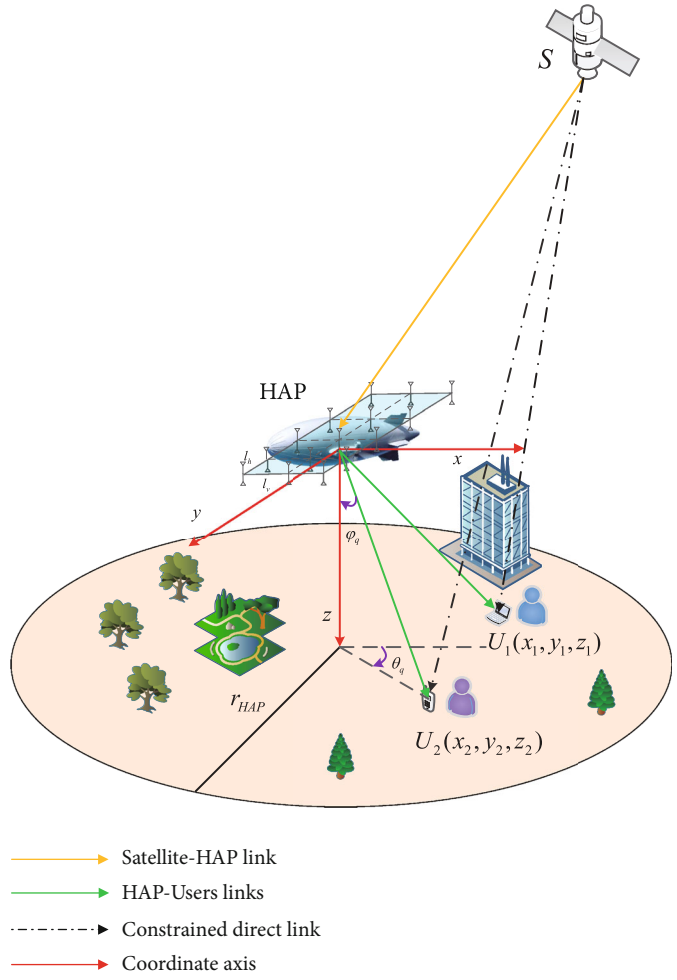

Figure 1: System model of NOMA-enabled ISATN.

power allocation coefficient of different signal satisfying $a_1 + a_2 = 1$. It is assumed that requirements for the quality of service (QoS) of U_1 is higher than U_2, (U_1 requires fast and low-rate connections, such as IoT sensors. U_2 is a high-resolution online game or video user which requires a continuous high-speed connection [20].) hence, U_1 is allocated with more power, i.e., $a_1 > a_2$. At HAP, the received signal can be denoted as

$$y_A = \sqrt{P_S} h_{\mathrm{SA}} w^H (\sqrt{a_a} x_1 + \sqrt{a_2} x_2) + w^H n_A, \tag{2}$$

where h_{SA} is the channel response of satellite to aerial link, which follows SR fading. To obtain the best system performance, maximum ratio combining (MRC) scheme is utilized in the considered system model which obeys $w = h_{\mathrm{SA}}/\|h_{\mathrm{SA}}\|$. w is the MRC weight vector at HAP due to N_r receive antennas. P_S denotes the transmit power of satellite. n_A is the addictive white Gaussian noise (AWGN) vector at aerial relay modeled as $n_H \sim \mathrm{CN}(0, \sigma^2_{\mathrm{SA}} I_{N_r \times 1})$.

In the next time slot, HAP relay utilizes DF and SIC protocol to decode and forward the received signal to the two terrestrial destinations [20, 32]. Notably, TAS scheme is adopted in HAP to balance the system performance and complexity. The received signal at U_i can be denoted as

$$y_{U_i} = \sqrt{P_A} h_{A_j, U_i} (\sqrt{a_1} x_1 + \sqrt{a_2} x_2) + n_{U_i}, \tag{3}$$

where h_{A_j, U_i} is the channel response of HAP-to-U_i links modeled as Nakagami-m fading. P_A represents the transmit power at aerial relay. n_{U_i} expresses the AWGN at U_i distributed as $n_{U_i} \sim CN(0, \sigma^2_{A_j, U_i})$.

In the channel estimation process, imperfect CSI and the limited estimation technology will result in CEEs inevitably. Utilizing the similar method in [7], CEE is often calculated by linear minimum mean-square error (MMSE). On this foundation, the estimated channel can be expressed as

$$\tilde{h}_T = h_T - e_T, \tag{4}$$

where $T \in \{\mathrm{SA}, A_j, U_i\}$. $e_T \sim \mathrm{CN}(0, \bar{v}_e)$ denotes the CEEs. With the help of [7], the variance can be given by

$$\bar{v}_e = E\{|h_T|^2\} - E\left\{\left|\tilde{h}_T\right|^2\right\} = \frac{1}{L_T \bar{V}_T + 1}, \tag{5}$$

where $\bar{V}_T = E\{V_T\} = P_T E\{|h_T|^2\}/\sigma_T^2$, P_T is the power of training symbols satisfying $P_T = (1-\phi)P_{\text{total}}$, P_{total} is the total transmission power and $\phi \in (0,1)$ is the power coefficient. L_T represents the pilot symbols length for channel estimation.

In the signal decoding under NOMA scheme, imperfect SIC is considered for weak performance of receiver [33]. Therefore, when the receiver decodes the signal x_2 with less power, the residual signal x_1 which does not completely eliminate is viewed as interference [30]. At the same time, considering CEEs, the signal-to-interference-plus-noise ratio (SINR) of different signals at aerial relay is denoted, correspondingly, as

$$\gamma_{A-1} = \frac{\phi a_1 \gamma_{\text{SA}}}{\phi a_2 \gamma_{\text{SA}} + \phi \bar{v}_e + 1}, \tag{6}$$

$$\gamma_{A-2} = \frac{\phi a_2 \gamma_{\text{SA}}}{\phi \xi a_1 \gamma_{\text{SA}} + \phi \bar{v}_e + 1}, \tag{7}$$

where $\gamma_{\text{SA}} = P_{\text{total}}\|\tilde{h}_{SA}\|^2/\sigma_{\text{SA}}^2 = \bar{\gamma}_{\text{SA}}\|\tilde{h}_{\text{SA}}\|^2$, $\xi \in (0,1)$ represents imperfect SIC coefficient.

Similarly, the SINR of two signals at U_i can be given by

$$\begin{aligned}
\gamma_1 &= \frac{\phi a_1 \gamma_{A_j,U_1}}{\phi a_2 \gamma_{A_j,U_1} + \phi \bar{v}_e + 1}, \\
\gamma_{2-1} &= \frac{\phi a_1 \gamma_{A_j,U_2}}{\phi a_2 \gamma_{A_j,U_2} + \phi \bar{v}_e + 1}, \\
\gamma_2 &= \frac{\phi a_2 \gamma_{A_j,U_2}}{\phi \xi a_1 \gamma_{A_j,U_2} + \phi \bar{v}_e + 1},
\end{aligned} \tag{8}$$

where $\gamma_{A_j,U_i} = P_{\text{total}}\|\tilde{h}_{A_j,U_i}\|^2/\sigma_{A_j,U_i}^2 = \bar{\gamma}_{A_j,U_i}\|\tilde{h}_{A_j,U_i}\|^2$.

2.2. Channel Models

2.2.1. Satellite to Aerial Link. The fading amplitude of SR channel response h_l, $1 \le l \le N_r$ can be expressed as [34].

$$h_l = C_{\text{SA}} g_l, \tag{9}$$

where g_l represents the channel coefficient of SR fading. C_{SA} denotes the path-loss factor in the satellite to aerial link that can be defined as

$$C_{\text{SA}} = \frac{\lambda \sqrt{G_{\text{S,SA}} G_{A,\text{SA}}}}{4\pi d_{\text{SA}} \sqrt{K_B \tau B}}, \tag{10}$$

where λ represents carrier wavelength. d_{SA} is the distance between satellite and aerial. $K_B = 1.380649 \times 10^{-23} J/K$ is the Boltzmann constant. τ denotes the transmission noise temperature. B is signal bandwidth. $G_{\text{S,SA}}$ is the satellite antenna gain which can be denoted as

$$G_{\text{S,SA}} = G_{\max}^S \left(\frac{J_1(k)}{2k} + 36 \frac{J_3(k)}{k^3} \right)^2, \tag{11}$$

where $G_{\max}^S$ is the maximum satellite antenna gain. $k = 2.07123 \sin\eta / \sin\eta_{3dB}$, η denotes the angle of the satellite center beam and the UPA of HAP. J_i denotes the first-kind Bessel function of order i. $G_{A,\text{SA}}$ is the HAP receive antenna gain which is defined as

$$G_{A,\text{SA}} \simeq \begin{cases} G_{\max}^A, & 0^\circ < \varphi < 1^\circ, \\ 32 - 25\log\varphi, & 1^\circ < \varphi < 48^\circ, \\ -10, & 48^\circ < \varphi < 180^\circ, \end{cases} \tag{12}$$

where $G_{\max}^A$ is the maximum gain of aerial relay receive antenna. φ is the off-boresight angle.

Without loss of generality, we assume that satellite to aerial link follows independent and identically distributed (i.i.d.) SR fading distribution [7]. According to $\gamma_{\text{SA}} = \bar{\gamma}_{\text{SA}} C_{\text{SA}}^2 \|g_{\text{SA}}\|^2$ and $\|g_{\text{SA}}\| = [g_1, g_2, \cdots, g_{N_r}]^T$, the probability density function (PDF) of γ_{SA} can be shown by [34].

$$f_{\gamma_{\text{SA}}}(x) = \sum_{k_1=0}^{m-1} \cdots \sum_{k_{N_r}=0}^{m-1} \Xi(N_r) \frac{x^{\Lambda_{N_r}-1} e^{-\Delta_{\text{SA}} x}}{\bar{\gamma}_{\text{SA}}{}^{\Lambda_{N_r}}}, \tag{13}$$

where

$$\Xi(N_r)\Delta = \prod_{j=1}^{N_r} \alpha_j \zeta(k_j) \prod_{j=1}^{N_r-1} B\left(\sum_{l=1}^{j} j + k_l, 1 + k_{j+1} \right), \tag{14}$$

and $B(.,.)$ represents beta function [[31], Eq. 8.384.1]. $\zeta(k_j) = (-1)^{k_j}(1-m)_{k_j}\delta^{k_j}/(k_j!)^2$, $(\cdot)_{k_j}$ denotes the Pochhammer symbol. $\Lambda_{N_r}\Delta = \sum_{j=1}^{N_r} k_j + N_r$, $\Delta_{\text{SA}} = \beta - \delta/\bar{\gamma}_{\text{SA}}$. $\alpha\Delta = (2\text{bm}/2\text{bm} + \Omega)^m/2b, \beta = {}^{\Delta}1/2b, \delta = {}^{\Delta}\Omega/2b(2\text{bm} + \Omega)$, $m \in (0,\infty)$, Ω, and $2b$ are the fading severity parameter, average power of the line-of-sight (LOS) component, and the multipath component, respectively.

By utilizing the similar method of [[31], Eq. 3.351.2], the cumulative distribution function (CDF) of γ_{SA} can be obtained as

$$F_{\gamma_{\text{SA}}}(x) = 1 - \sum_{k_1=0}^{m-1} \cdots \sum_{k_{N_r}=0}^{m-1} \sum_{t=0}^{\Lambda_{N_r}-1} \frac{\Xi(N_r)(\Lambda_{N_r}-1)!}{t! \Delta_{\text{SA}}^{\Lambda_{N_r}-t} \bar{\gamma}_{\text{SA}}{}^{\Lambda_{N_r}}} x^t e^{-\Delta_{\text{SA}} x}. \tag{15}$$

2.2.2. Aerial to U_i Links. The channel of aerial to U_i links undergoes Nakagami-m fading, which can be given by [32].

$$h_{A_j,U_i} = C_{A_j,U_i} g_{A_j,U_i} \partial(\varphi_i, \theta_i), \tag{16}$$

where g_{A_j,U_i} represents the channel coefficient of Nakagami-m fading. C_{A_j,U_i} is the path-loss factor in the aerial to U_i links that can be expressed as

$$C_{A_j,U_i} = G_{A_j} + G_{U_i} + \frac{1}{2}\left[20 \lg (\lambda/4\pi) - 10\varsigma \lg d_{AU_i}\right], \quad (17)$$

where G_{A_j} and G_{U_i} are the antenna gain of HAP relay and users, correspondingly. ς represents the path loss value and d_{AU_i} is the distance between aerial and users.

Moreover, we set a spatial coordinate system with aerial relay as the origin in Figure 1, $\theta_i \in [0, 2\pi)$ is the azimuth between aerial and users, and $\varphi_i \in [0, \pi/2)$ is the elevation from aerial to users. $\partial(\varphi_i, \theta_i)$ shows the array steering matrix [32, 35], which is defined as

$$\partial(\varphi_i, \theta_i) = \partial_x(\varphi_i, \theta_i) \otimes \partial_y(\varphi_i, \theta_i), \quad (18)$$

where $\partial_x(\varphi_i, \theta_i)$ and $\partial_y(\varphi_i, \theta_i)$ are the horizontal and vertical antennas steering vectors, which can be given by

$$\begin{aligned}\partial_x(\varphi_i, \theta_i) &= \left[e^{-j(2\pi l_v/\lambda)(1-(N_h+1)/2)\cos\varphi_i\cos\theta_i}, \cdots, e^{-j(2\pi l_v/\lambda)(N_h-(N_h+1)/2)\cos\varphi_i\cos\theta_i}\right]^T,\\ \partial_y(\varphi_i, \theta_i) &= \left[e^{-j(2\pi l_h/\lambda)(1-(N_v+1)/2)\cos\varphi_i\cos\theta_i}, \cdots, e^{-j(2\pi l_h/\lambda)(N_v-(N_v+1)/2)\cos\varphi_i\cos\theta_i}\right]^T,\end{aligned} \quad (19)$$

where $N_h \times N_v = N_t$, N_h, and l_h are the number and interelement distance of horizontal antennas. N_v and l_v are the number and interelement distance of vertical directions.

Finally, on the basis of three-dimensional coordinates, φ_i and θ_i are, respectively, expressed as

$$\begin{aligned}\varphi_i &= \arctan(),\\ \theta_i &= \begin{cases} \arccos\left(\dfrac{x_i}{\sqrt{x_i^2 + y_i^2}}\right), & y_i \geq 0,\\ 2\pi - \arccos\left(\dfrac{z_i}{\sqrt{x_i^2 + y_i^2}}\right), & y_i < 0,\end{cases}\end{aligned} \quad (20)$$

According to $\gamma_{A_j,U_i} = \bar{\gamma}_{A_j,U_i} C^2_{A_j,U_i} [\partial(\varphi_i, \theta_i)]^2 \| g_{A_j,U_i} \|^2$, the PDF and CDF of γ_{A_j,U_i} are given by

$$\begin{aligned} f_{\gamma_{A_j,U_i}}(x) &= \frac{\Theta_i^{m_i}}{\Gamma(m_i)} x^{m_i-1} e^{-\Theta_i x},\\ F_{\gamma_{A_j,U_i}}(x) &= 1 - e^{-\Theta_i x} \sum_{k=0}^{m_i-1} \frac{\Theta_i^k x^k}{k!},\end{aligned} \quad (21)$$

where $\Theta_i = m_i/\Omega_i \bar{\gamma}_{A_j,U_i}$. m_i is the fading severity factor and Ω_i denotes the average power.

3. Performance Analysis

Based on the requirements of different users, we propose two TAS schemes to enhance the performance of our proposed NOMA-enabled ISATN and reduce system complexity. Then, the expressions for EC are derived to manifest the impacts of different schemes under imperfect CSI and SIC.

3.1. Transmit Antenna Selection (TAS) Schemes. Two TAS schemes, i.e., TAS1 and TAS2 schemes, are presented to improve the performance of different U_i and reduce the complexity of the whole system. For TAS1 scheme, U_1 needs better service quality, thus, the optimal antenna $j*$ is selected to transmit the superimposed signal to U_1, which can be expressed as

$$j* = \underbrace{\operatorname{argmax}}_{j\in\{1,2,\cdots,N_t\}} \left\{\gamma_{A_j,U_1}\right\}, \quad (22)$$

meanwhile, a random antenna is chosen to transmit the signal to U_2.

For TAS2 scheme, U_2 needs better service quality, hence, we choose the best antenna $j*$ to transmit the superimposed signal to U_2, which can be denoted as

$$j* = \underbrace{\operatorname{argmax}}_{j\in\{1,2,\cdots,N_t\}} \left\{\gamma_{A_j,U_2}\right\}, \quad (23)$$

meanwhile, a random antenna is selected to transmit the signal to U_1.

From the above two schemes and with the help of multinomial theorem [21], the CDF of Nakagami-m fading is derived as

$$F_{\gamma_{A_{j*},U_i}}(x) = \left[F_{\gamma_{A_j,U_i}}(x)\right]^{N_t} = \sum_{t=0}^{N_t} \binom{N_t}{t} \left(-e^{-\Theta_i x}\right)^t \Phi(x), \quad (24)$$

where $\Phi(x) = \sum_{t_i\geq 0, t_0+t_1+\cdots+t_{m_i-1}=t} t! \prod_{0\leq l\leq m_i} \left(\Theta_i^l x^l / l!\right)^{t_l} / t_0!\, t_1! \cdots t_{m_i-1}!$.

Through derivations and order statistics, the PDF of Nakagami-m fading under TAS scheme can be obtained as

$$f_{\gamma_{A_{j*},U_i}}(x) = N_t f_{\gamma_{A_j,U_i}}(x)\left[F_{\gamma_{A_j,U_i}}(x)\right]^{N_t-1}. \tag{25}$$

3.2. Ergodic Capacity. EC is a key merit to analyze the performance of the considered ISATN. The EC of the ISATN defines the time average of the capacity on the satellite to aerial link and aerial to users' links [30]. Due to the ISATN consists two phases, the overall EC can be denoted as

$$\mathrm{EC} = \min\left[\mathrm{EC}_{\mathrm{SA}}, \mathrm{EC}_{\mathrm{AU}}\right], \tag{26}$$

where $\mathrm{EC}_{\mathrm{SA}}$ and $\mathrm{EC}_{\mathrm{AU}}$ are the EC of the two links, respectively.

In the first time slot, $\mathrm{EC}_{\mathrm{SA}}$ is defined as the sum of average instantaneous mutual information of the end-to-end SINR at HAP, according to (6) and (7), the expression can be written as.

$$\mathrm{EC}_{\mathrm{SA}} = \frac{1}{2}\left\{E[\log_2(1+\gamma_{A-1})] + E[\log_2(1+\gamma_{A-2})]\right\}, \tag{27}$$

where 1/2 is generated because of half duplex DF relaying protocol.

After necessary manipulation transformation, $\mathrm{EC}_{\mathrm{SA}}$ can be obtained as

$$\begin{aligned}\mathrm{EC}_{\mathrm{SA}} = \frac{1}{2\ln 2}\Bigg\{&E\left[\ln\left(\frac{\gamma_{\mathrm{SA}}\phi}{\phi\bar{\nu}_e+1}+1\right)\right] - E\left[\ln\left(\frac{\gamma_{SA}\phi a_2}{\phi\bar{\nu}_e+1}+1\right)\right]\\ &+E\left[\ln\left(\frac{\gamma_{\mathrm{SA}}\phi(a_2+\xi a_1)}{\phi\bar{\nu}_e+1}+1\right)\right] - E\left[\ln\left(\frac{\gamma_{\mathrm{SA}}\phi\xi a_1}{\phi\bar{\nu}_e+1}+1\right)\right]\Bigg\}.\end{aligned} \tag{28}$$

Table 1: System parameters.

Parameter name	Parameter value
HAP height	20 km
Frequency	2 GHz
Bandwidth	15 MHz
Noise temperature	300 K
dB angle	0.5°
Beam gain	48 dB
Antenna gain	4 dB

Let $\gamma_{\mathrm{SA}} = x$, $\gamma_{\mathrm{SA}}\phi/\phi\bar{\nu}_e + 1 = z_1$, $\gamma_{\mathrm{SA}}\phi a_2/\phi\bar{\nu}_e + 1 = z_2$, $\gamma_{\mathrm{SA}}\phi(a_2+\xi a_1)/\phi\bar{\nu}_e + 1 = z_3$, and $\gamma_{\mathrm{SA}}\phi\xi a_1/\phi\bar{\nu}_e + 1 = z_4$, with the help of probability transformation formula, the PDF of z_1 can be calculated as

$$f_{z_1}(z) = \frac{\phi\bar{\nu}_e+1}{\phi} f_x\left(\frac{\phi\bar{\nu}_e+1}{\phi}z\right). \tag{29}$$

On the basis of (13), (29) can be reexpressed as

$$f_{z_1}(z) = \sum_{k_1=0}^{m-1}\cdots\sum_{k_{N_t}=0}^{m-1}\Xi(N_t)\left(\frac{\phi\bar{\nu}_e+1}{\phi}\right)^{\Lambda_{N_t}-1}\frac{z^{\Lambda_{N_t}-1}e^{-\Delta_{SA}\phi\bar{\nu}_e+1/\phi z}}{\bar{\gamma}_{SA}{}^{\Lambda_{N_t}}}. \tag{30}$$

Furthermore, the EC of the ISATN can be rewritten as

$$\mathrm{EC}_{\mathrm{SA}} = \frac{1}{2\ln 2}\times\Bigg\{\underbrace{\int_0^\infty \ln(z+1)f_{z_1}(z)dz}_{S_1} - \underbrace{\int_0^\infty \ln(z+1)f_{z_2}(z)dz}_{S_2} + \underbrace{\int_0^\infty \ln(z+1)f_{z_3}(z)dz}_{S_3} - \underbrace{\int_0^\infty \ln(z+1)f_{z_4}(z)dz}_{S_4}\Bigg\}. \tag{31}$$

With the help of [[36], Eq.8.4.6.5], then we utilize Meijer-G function [[31], Eq. 9.301] to further deduce EC, namely,

$$\ln(1+z) = G_{22}^{12}\left(z\middle|\begin{matrix}1, & 1\\ 1 & 0\end{matrix}\right). \tag{32}$$

By substituting (30) and (32) into S_1, with the aid of [[36], Eq.2.24.3.1] and [[36], Eq.8.2.2.14], S_1 can be expressed as

$$S_1 = \sum_{k_1=0}^{m-1}\cdots\sum_{k_{N_t}=0}^{m-1}\frac{\Xi(N_t)}{\bar{\gamma}_{SA}{}^{\Lambda_{N_t}}\Delta_{SA}{}^{\Lambda_{N_t}}}G_{23}^{31}\left(\frac{(\phi\bar{\nu}_e+1)\Delta_{SA}}{\phi}\middle|\begin{matrix}0, & 1\\ \Lambda_{N_t}, & 1,0\end{matrix}\right). \tag{33}$$

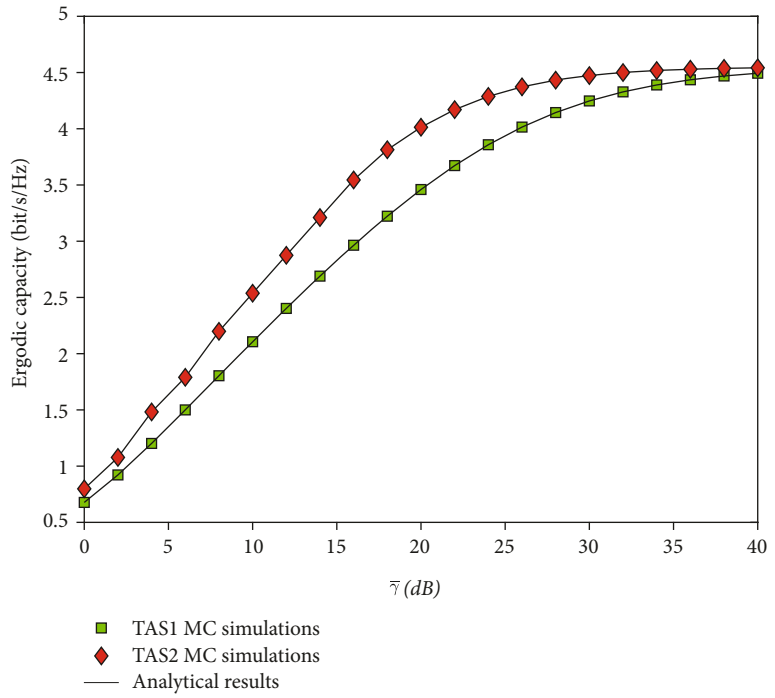

(a)

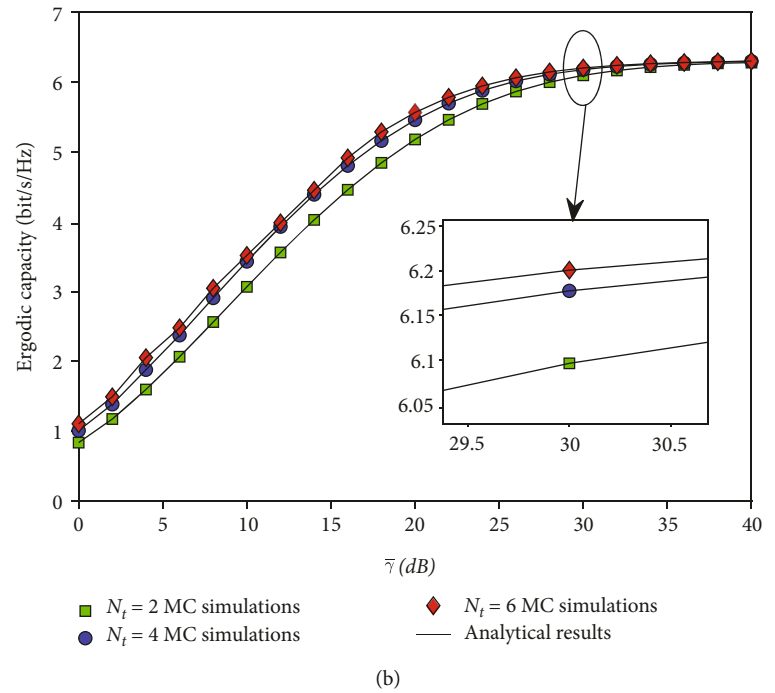

(b)

Figure 2: EC versus $\bar{\gamma}$ with different TAS designs. (a) EC with different TAS schemes. (b) EC with different transmit antenna numbers.

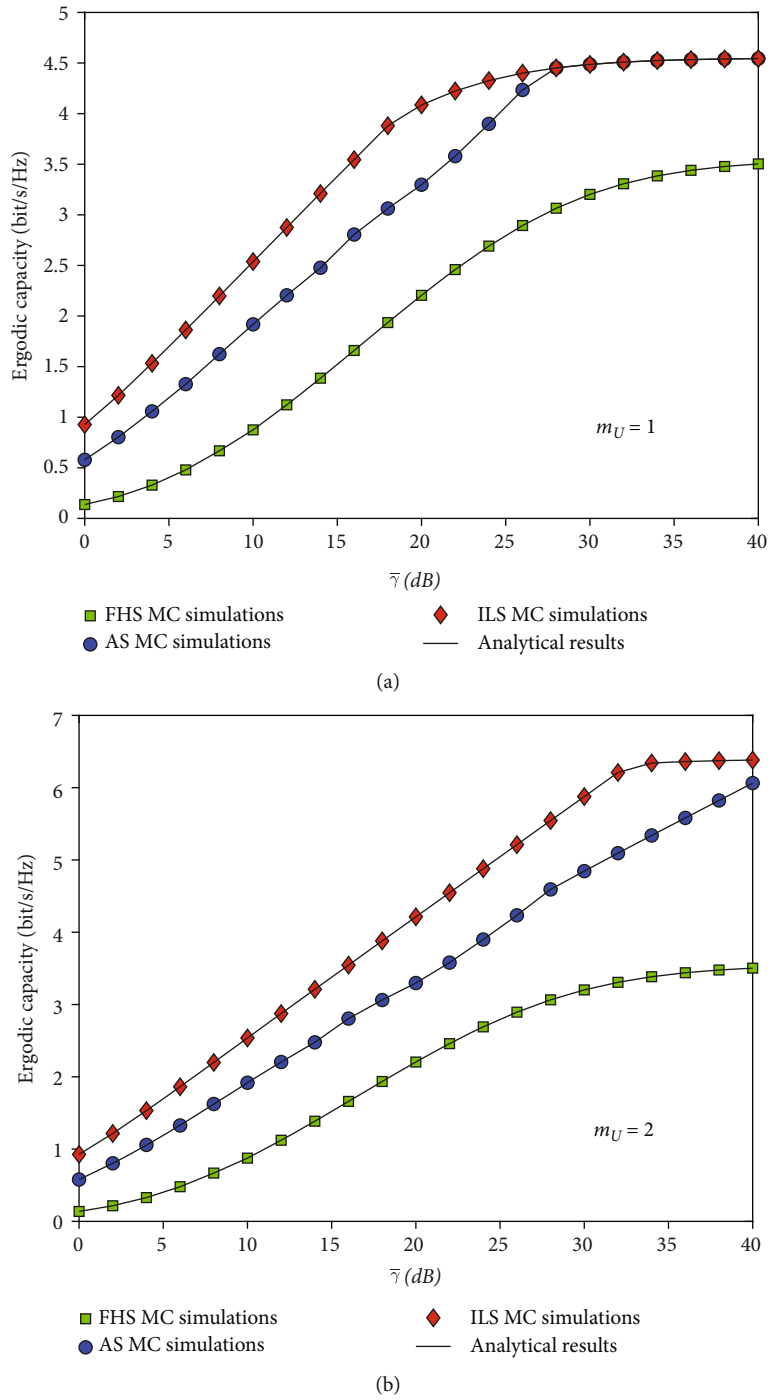

Figure 3: EC versus different fading parameters. (a) Nakagami-m: $m_U = 1$. (b) Nakagami-m: $m_U = 2$.

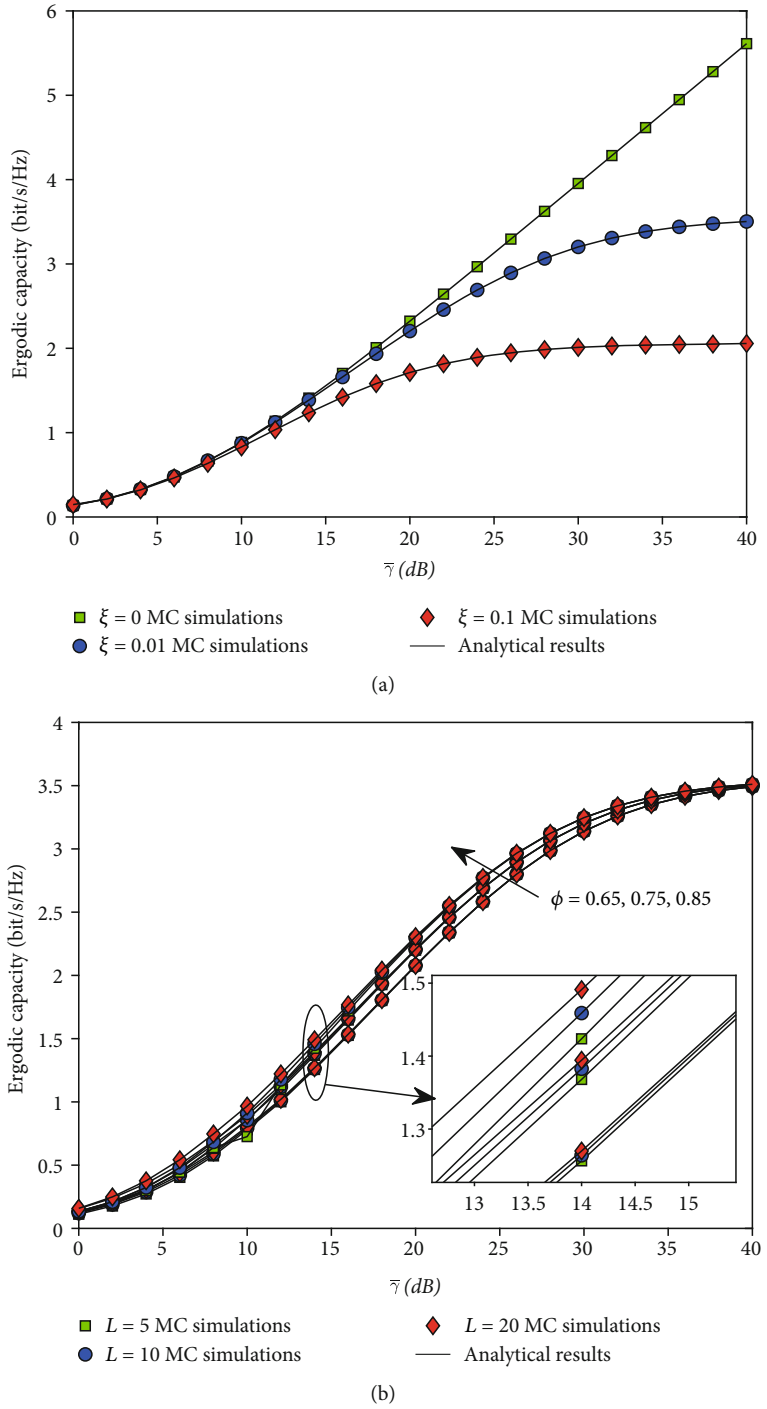

Figure 4: EC versus different imperfections. (a) EC with different imperfect SIC. (b) EC with different CEEs conditions.

With the similar way, we can also get the expressions of S_2, S_3, and S_4 as follows:

$$S_2 = \sum_{k_1=0}^{m-1} \cdots \sum_{k_{N_t}=0}^{m-1} \frac{\Xi(N_t)}{\bar{\gamma}_{\mathrm{SA}}^{\Lambda_{N_t}} \Delta_{\mathrm{SA}}^{\Lambda_{N_t}}} G_{23}^{31}\left(\frac{(\phi\bar{\nu}_e+1)\Delta_{\mathrm{SA}}}{\phi a_2}\middle|\begin{matrix}0, & 1\\ \Lambda_{N_t}, & 1,0\end{matrix}\right),$$

$$S_3 = \sum_{k_1=0}^{m-1} \cdots \sum_{k_{N_t}=0}^{m-1} \frac{\Xi(N_t)}{\bar{\gamma}_{\mathrm{SA}}^{\Lambda_{N_t}} \Delta_{\mathrm{SA}}^{\Lambda_{N_t}}} G_{23}^{31}\left(\frac{(\phi\bar{\nu}_e+1)\Delta_{\mathrm{SA}}}{\phi(a_2+\xi a_1)}\middle|\begin{matrix}0, & 1\\ \Lambda_{N_t}, & 1,0\end{matrix}\right),$$

$$S_4 = \sum_{k_1=0}^{m-1} \cdots \sum_{k_{N_t}=0}^{m-1} \frac{\Xi(N_t)}{\bar{\gamma}_{\mathrm{SA}}^{\Lambda_{N_t}} \Delta_{\mathrm{SA}}^{\Lambda_{N_t}}} G_{23}^{31}\left(\frac{(\phi\bar{\nu}_e+1)\Delta_{\mathrm{SA}}}{\phi\xi a_1}\middle|\begin{matrix}0, & 1\\ \Lambda_{N_t}, & 1,0\end{matrix}\right). \tag{34}$$

By using them, the final expression of $\mathrm{EC}_{\mathrm{SA}}$ can be expressed as

$$\begin{aligned}\mathrm{EC}_{\mathrm{SA}} = \sum_{k_1=0}^{m-1} \cdots \sum_{k_{N_t}=0}^{m-1} \Xi(N_t) \frac{1}{\bar{\gamma}_{\mathrm{SA}}^{\Lambda_{N_t}} \Delta_{\mathrm{SA}}^{\Lambda_{N_t}}} \\ \cdot \left[G_{23}^{31}\left(\frac{\phi\bar{\nu}_e+1}{\phi}\Delta_{\mathrm{SA}}\middle|\begin{matrix}0, & 1\\ \Lambda_{N_t}, & 1, \quad 0\end{matrix}\right)\right. \\ - G_{23}^{31}\left(\frac{\phi\bar{\nu}_e+1}{\phi a_2}\Delta_{\mathrm{SA}}\middle|\begin{matrix}0, & 1\\ \Lambda_{N_t}, & 1, \quad 0\end{matrix}\right) \\ + G_{23}^{31}\left(\frac{\phi\bar{\nu}_e+1}{\phi(a_2+\xi a_1)}\Delta_{\mathrm{SA}}\middle|\begin{matrix}0, & 1\\ \Lambda_{N_t}, & 1, \quad 0\end{matrix}\right) \\ \left. - G_{23}^{31}\left(\frac{\phi\bar{\nu}_e+1}{\phi\xi a_1}\Delta_{\mathrm{SA}}\middle|\begin{matrix}0, & 1\\ \Lambda_{N_t}, & 1, \quad 0\end{matrix}\right)\right].\end{aligned} \tag{35}$$

Applying the same method, the expression of $\mathrm{EC}_{\mathrm{AU}}$ under TAS1 scheme can be derived as

$$\begin{aligned}\mathrm{EC}_{\mathrm{AU}}^{\mathrm{TAS1}} = \frac{1}{2\ln 2}\left\{\frac{1}{\Gamma(m_2)}\left[G_{23}^{31}\left(\frac{\phi\bar{\nu}_e+1}{\phi}\Theta_2\middle|\begin{matrix}0, & 1\\ m_2, & 0,0\end{matrix}\right)\right.\right. \\ - G_{23}^{31}\left(\frac{\phi\bar{\nu}_e+1}{\phi a_2}\Theta_2\middle|\begin{matrix}0, & 1\\ m_2, & 0,0\end{matrix}\right) \\ + G_{23}^{31}\left(\frac{\phi\bar{\nu}_e+1}{\phi(a_2+\xi a_1)}\Theta_2\middle|\begin{matrix}0, & 1\\ \mathrm{m}_2, & 0,0\end{matrix}\right) \\ \left.\left. - G_{23}^{31}\left(\frac{\phi\bar{\nu}_e+1}{\phi\xi a_1}\Theta_2\middle|\begin{matrix}0, & 1\\ m_2, & 0,0\end{matrix}\right)\right] \right. \\ + N_t \frac{\Theta_1^{m_1}}{\Gamma(m_1)} \sum_{t=0}^{N_t-1}\binom{N_t-1}{t}(-1)^t \sum_{t_i\geq 0, t_0+t_1+\cdots+t_{m_1-1}=t} \frac{t!}{t_0!t_1!\cdots t_{m_1-1}!} \prod_{0\leq l\leq m_1}\left(\frac{\Theta_1^{\,l}}{l!}\right)^{t_l} \\ \times [\Theta_1(t+1)]^{-(l\times t_l+m_1)}\left[G_{23}^{31}\left(\frac{\Theta_1(t+1)(\phi\bar{\nu}_e+1)}{\phi}\middle|\begin{matrix}0, 1\\ l\times t_l+m_1, 0, 0\end{matrix}\right)\right. \\ \left.\left. - G_{23}^{31}\left(\frac{\Theta_1(t+1)(\phi\bar{\nu}_e+1)}{\phi a_2}\middle|\begin{matrix}0, 1\\ l\times t_l+m_1, 0, 0\end{matrix}\right)\right]\right\}.\end{aligned} \tag{36}$$

Finally, by substituting (35) and (36) into (26), the overall EC of the NOMA-enabled ISATNs under TAS1 is obtained.

Applying the similar derivations, the expression of overall EC under TAS2 can be obtained. Owing to the limitations of page length, this step is omitted.

4. Numerical Results

In this section, Monte Carlo (MC) simulations are performed to verify our theoretical derivations. In general, we set $\bar{\gamma}_{\mathrm{SA}} = \bar{\gamma}_{A_j,U_i} = \bar{\gamma}$, $m_1 = m_2 = m_U$, and $\Omega_1 = \Omega_2 = 1$. Frequent heavy shadowing (FHS), average shadowing (AS), and infrequent light shadowing (ILS) are given as $\{m, b, \Omega\} = \{1{,}0.063{,}0.0007\}$, $\{5{,}0.251{,}0.279\}$, and $\{10{,}0.158{,}1.29\}$, respectively. The rest system values are shown in Table 1 [32].

Figure 2 depicts the EC versus $\bar{\gamma}$ with different TAS designs under $\xi = 0.01, L = 5, \sigma = 0.75, m_U = 1$ and ILS. Firstly, we can obviously see that the analytical results are in line with simulation results, which verifies the effectiveness of the theoretical derivations. Apparently, Figure 2(a) shows that the EC under TAS2 scheme is superior to that under TAS1 scheme, which can be explained by the fact that the selected best antenna under TAS2 scheme is employed to transmit superimposed signal to the user with less power in NOMA scheme. Thus, the overall achievable system performance is enhanced. In addition, Figure 2(b) plots the overall EC of the system improves with transmit antenna number. The more antennas the system has, the more suitable antenna can be selected to transmit signals. Besides, EC tends to be steady with the increase of $\bar{\gamma}$.

Figure 3 compares the EC versus $\bar{\gamma}$ with different SR fading and Nakagami-m fading parameters under $\xi = 0.01$, $L = 5, \sigma = 0.75, N_t = 6$ and TAS1 scheme. It can be clearly seen in Figure 3 that the overall EC enhances gradually along with the improvement of SR fading channel conditions. However, the performance of overall EC is limited due to the second time slot. When $m_U = 1$, the upper limit of EC is 4.544. When $m_U = 2$, the upper limit of EC is 6.382. Likewise, the overall EC improves in high SNR regime with the improvement of Nakagami-m fading channel conditions.

Figure 4 shows the EC versus $\bar{\gamma}$ with different imperfections under $N_t = 6, m_U = 1$, FHS, and TAS1 scheme. From Figure 4(a), it can be seen that the EC is sensitive to the different imperfect SIC conditions. The upper limit of EC is 5.612 under perfect SIC. When $\xi = 0.1$, the upper limit of EC is only 2.057. The EC of the considered ISATN becomes worse with the increase of ξ, which can be explained the NOMA users employ SIC technique to decode the superimposed signal at the receiver. When the SIC does not work perfectly, the reception performance of the system directly decline, leading to the reduction of the overall EC for the system. Besides, from Figure 4(b), as the growth of L and ϕ, the CEEs of the NOMA-enabled ISATN get smaller, which results in improvement of EC. However, when the average SNR $\bar{\gamma}$ increases and exceeds 40 dB, the impact of imperfect CSI is reduced, and several curves gradually overlap.

5. Conclusions

In this paper, the EC performance of a NOMA-enabled ISATN was investigated with two TAS schemes under

imperfect CSI and SIC. Firstly, we deployed a NOMA-enabled ISATN with the help of HAP. Next, two TAS schemes were proposed to balance system performance and complexity in detail. By assuming that imperfect CSI and SIC occurred in the considered system, exact closed-form expressions for overall EC of the ISATN were obtained. Finally, through the MC simulations, we validated the superiority of the performance for our proposed TAS2 schemes. Besides, imperfect CSI and SIC seriously degraded the performance of the system, which is instructive for engineering practice.

Data Availability

No data were used to support this study.

Conflicts of Interest

The authors declare that they have no conflicts of interest regarding the publication of this article.

Acknowledgments

This work was supported by the National Science Foundation of China under grants 62001517. Thanks are due to all the authors for their contribution to this paper.

References

[1] M. Lin, Q. Huang, T. de Cola et al., "Integrated 5G-satellite networks: a perspective on physical layer reliability and security," *IEEE Wireless Communications*, vol. 27, no. 6, pp. 152–159, 2020.

[2] B. Li, Z. Fei, C. Zhou, and Y. Zhang, "Physical-layer security in space information networks: a survey," *IEEE Internet of Things Journal*, vol. 7, no. 1, pp. 33–52, 2020.

[3] W. Wu, F. Zhou, R. Q. Hu, and B. Wang, "Energy-efficient resource allocation for secure NOMA-enabled mobile edge computing networks," *IEEE Transactions on Communications*, vol. 68, no. 1, pp. 493–505, 2020.

[4] K. Guo and K. An, "On the performance of RIS-assisted integrated satellite-UAV-terrestrial networks with hardware impairments and interference," *IEEE Wireless Communications Letters*, vol. 11, no. 1, pp. 131–135, 2022.

[5] X. Li, M. Zhao, Y. Liu, L. Li, Z. Ding, and A. Nallanathan, "Secrecy analysis of ambient backscatter NOMA systems under I/Q imbalance," *IEEE Transactions on Vehicular Technology*, vol. 69, no. 10, pp. 12286–12290, 2020.

[6] X. Yue, Z. Qin, Y. Liu, S. Kang, and Y. Chen, "A unified framework for non-orthogonal multiple access," *IEEE Transactions on Communications*, vol. 66, no. 11, pp. 5346–5359, 2018.

[7] N. Zhao, Y. Li, S. Zhang et al., "Security enhancement for NOMA-UAV networks," *IEEE Transactions on Vehicular Technology*, vol. 69, no. 4, pp. 3994–4005, 2020.

[8] Z. Lin, M. Lin, J. B. Wang, T. de Cola, and J. Wang, "Joint beamforming and power allocation for satellite-terrestrial integrated networks with non-orthogonal multiple access," *IEEE Journal on Selected Topics in Signal Processing*, vol. 13, no. 3, pp. 657–670, 2019.

[9] Y. Tian, G. Pan, M. A. Kishk, and M. S. Alouini, "Stochastic analysis of cooperative satellite-UAV communications," *IEEE Transactions on Wireless Communications*, vol. 21, no. 6, pp. 3570–3586, 2022.

[10] Q. Wang, X. Li, S. Bhatia et al., "UAV-enabled non-orthogonal multiple access networks for ground-air-ground communications," *IEEE Transactions on Green Communications and Networking*, vol. 6, no. 3, pp. 1340–1354, 2022.

[11] H. Zhang, G. Pan, S. Ke, S. Wang, and J. An, "Outage analysis of cooperative satellite-aerial-terrestrial networks with spatially random terminals," *IEEE Transactions on Communications*, vol. 70, no. 7, pp. 4972–4987, 2022.

[12] V. Bankey and P. K. Upadhyay, "Physical layer security of multiuser multirelay hybrid satellite-terrestrial relay networks," *IEEE Transactions on Vehicular Technology*, vol. 68, no. 3, pp. 2488–2501, 2019.

[13] R. Liu, K. Guo, K. An, S. Zhu, and H. Shuai, "NOMA-based integrated satellite-terrestrial relay networks under spectrum sharing environment," *IEEE Wireless Communications Letters*, vol. 10, no. 6, pp. 1266–1270, 2021.

[14] M. Jia, X. Wang, Q. Guo, I. W. H. Ho, X. Gu, and F. C. M. Lau, "Performance analysis of cooperative non-orthogonal multiple access based on spectrum sensing," *IEEE Transactions on Vehicular Technology*, vol. 68, no. 7, pp. 6855–6866, 2019.

[15] X. Yue, Y. Liu, S. Kang, A. Nallanathan, and Y. Chen, "Modeling and analysis of two-way relay non-orthogonal multiple access systems," *IEEE Transactions on Communications*, vol. 66, no. 9, pp. 3784–3796, 2018.

[16] X. Li, M. Zhao, M. Zeng et al., "Hardware impaired ambient backscatter NOMA systems: reliability and security," *IEEE Transactions on Communications*, vol. 69, no. 4, pp. 2723–2736, 2021.

[17] X. Yan, H. Xiao, C. Wang, and K. An, "Outage performance of NOMA-based hybrid satellite-terrestrial relay networks," *IEEE Wireless Communications Letters*, vol. 7, no. 4, pp. 538–541, 2018.

[18] V. Singh and P. K. Upadhyay, "Exploiting FD/HD cooperative-NOMA in underlay cognitive hybrid satellite-terrestrial networks," *IEEE Transactions on Cognitive Communications and Networking*, vol. 8, no. 1, pp. 246–262, 2022.

[19] K. Guo, M. Lin, B. Zhang, W. P. Zhu, J. B. Wang, and T. A. Tsiftsis, "On the performance of LMS communication with hardware impairments and interference," *IEEE Transactions on Communications*, vol. 67, no. 2, pp. 1490–1505, 2019.

[20] O. Maraqa, A. S. Rajasekaran, S. al-Ahmadi, H. Yanikomeroglu, and S. M. Sait, "A survey of rate-optimal power domain NOMA with enabling technologies of future wireless networks," *IEEE Communication Surveys and Tutorials*, vol. 22, no. 4, pp. 2192–2235, 2020.

[21] H. Lei, C. Gao, I. S. Ansari et al., "Secrecy outage performance of transmit antenna selection for MIMO underlay cognitive radio systems over Nakagami- m channels," *IEEE Transactions on Vehicular Technology*, vol. 66, no. 3, pp. 2237–2250, 2017.

[22] H. Shuai, K. Guo, K. An, Y. Huang, and S. Zhu, "Transmit antenna selection in NOMA-based integrated satellite-HAP-terrestrial networks with imperfect CSI and SIC," *IEEE Wireless Communications Letters*, vol. 11, no. 8, pp. 1565–1569, 2022.

[23] L. Lv, Q. Ye, Z. Ding, Z. Li, N. al-Dhahir, and J. Chen, "Multi-antenna two-way relay based cooperative NOMA," *IEEE Transactions on Wireless Communications*, vol. 19, no. 10, pp. 6486–6503, 2020.

[24] Y. Ruan, L. Jiang, Y. Li, and R. Zhang, "Energy-efficient power control for cognitive satellite-terrestrial networks with outdated CSI," *IEEE Systems Journal*, vol. 15, no. 1, pp. 1329–1332, 2021.

[25] S. Solanki, P. K. Upadhyay, D. B. da Costa, P. S. Bithas, A. G. Kanatas, and U. S. Dias, "Joint impact of RF hardware impairments and channel estimation errors in spectrum sharing multiple-relay networks," *IEEE Transactions on Communications*, vol. 66, no. 9, pp. 3809–3824, 2018.

[26] X. Li, J. Li, Y. Liu, Z. Ding, and A. Nallanathan, "Residual transceiver hardware impairments on cooperative NOMA networks," *IEEE Transactions on Wireless Communications*, vol. 19, no. 1, pp. 680–695, 2020.

[27] X. Yue, Y. Liu, Y. Yao et al., "Outage behaviors of NOMA-based satellite network over shadowed-rician fading channels," *IEEE Transactions on Vehicular Technology*, vol. 69, no. 6, pp. 6818–6821, 2020.

[28] B. K. S. Lima, D. B. da Costa, L. Yang, F. R. M. Lima, R. Oliveira, and U. S. Dias, "Adaptive power factor allocation for cooperative full-duplex NOMA systems with imperfect SIC and rate fairness," *IEEE Transactions on Vehicular Technology*, vol. 69, no. 11, pp. 14061–14066, 2020.

[29] X. Yue, Y. Liu, Y. Yao, X. Li, R. Liu, and A. Nallanathan, "Secure communications in a unified non-orthogonal multiple access framework," *IEEE Transactions on Wireless Communications*, vol. 19, no. 3, pp. 2163–2178, 2020.

[30] H. Shuai, R. Liu, S. Zhu, C. Li, and Y. Fang, "Ergodic capacity of NOMA-based multi-antenna LMS systems with imperfect limitations," *Sensors*, vol. 22, no. 1, p. 330, 2022.

[31] I. S. Gradshteyn, I. M. Ryzhik, A. Jeffrey, and D. Zwillinger, *Table of Integrals, Series and Products*, Elsevier, Amsterdam, Boston, 7th edition, 2007.

[32] Q. Huang, M. Lin, W. P. Zhu, J. Cheng, and M. S. Alouini, "Uplink massive access in mixed RF/FSO satellite-aerial-terrestrial networks," *IEEE Transactions on Communications*, vol. 69, no. 4, pp. 2413–2426, 2021.

[33] X. Li, M. Liu, C. Deng, P. T. Mathiopoulos, Z. Ding, and Y. Liu, "Full-duplex cooperative NOMA relaying systems with I/Q imbalance and imperfect SIC," *IEEE Wireless Communications Letters*, vol. 9, no. 1, pp. 17–20, 2020.

[34] K. Guo, C. Dong, and K. An, "NOMA-based cognitive satellite terrestrial relay network: secrecy performance under channel estimation errors and hardware impairments," *IEEE Internet of Things Journal*, vol. 9, no. 18, pp. 17334–17347, 2022.

[35] W. Feng, N. Zhao, S. Ao et al., "Joint 3D trajectory and power optimization for UAV-aided mmWave MIMO-NOMA networks," *IEEE Transactions on Communications*, vol. 69, no. 4, pp. 2346–2358, 2021.

[36] A. P. Prudnikov, Y. A. Brychkov, and O. I. Marichev, *Integrals and Series, Volume 3: More Special Functions*, Ser. Gordon and Breach, New York, 1990.